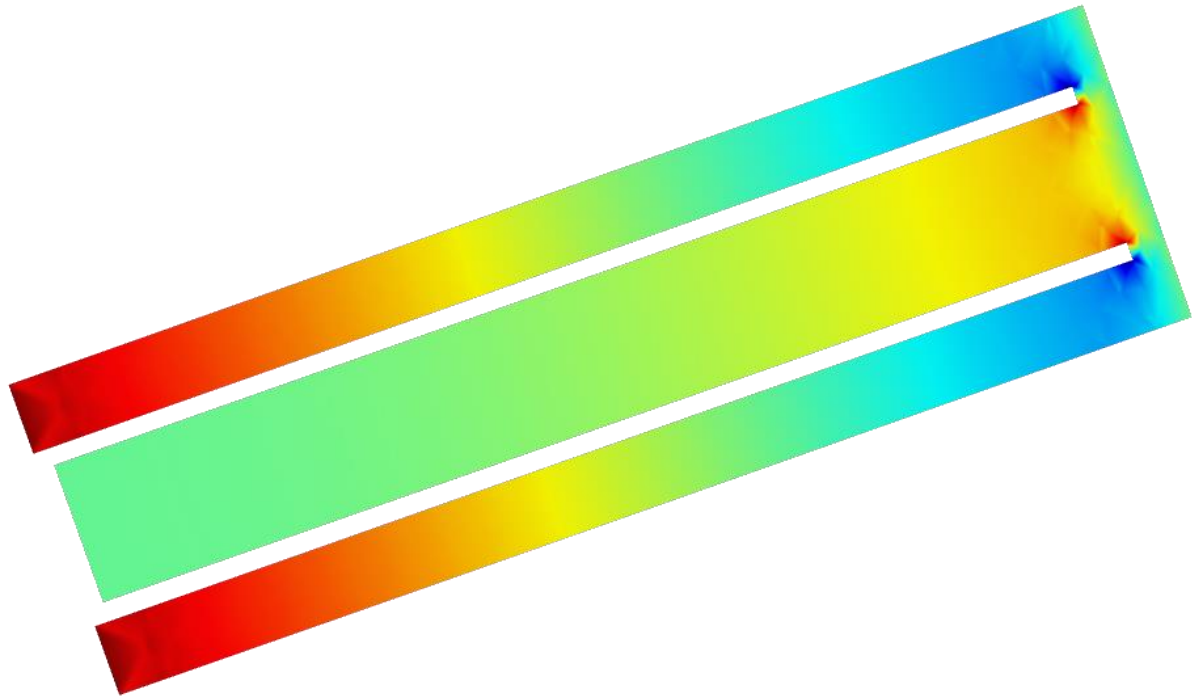




CHALMERS
UNIVERSITY OF TECHNOLOGY



Bandwidth Improvement of a Piezoelectric Micro Energy Harvester

Master's thesis in Applied Mechanics

JOHAN ANDERSSON

DEPARTMENT OF MECHANICS AND MARITIME SCIENCES

CHALMERS UNIVERSITY OF TECHNOLOGY
Göteborg, Sweden 2020
www.chalmers.se

MASTER'S THESIS IN APPLIED MECHANICS

Bandwidth Improvement of a Piezoelectric Micro Energy Harvester

JOHAN ANDERSSON



CHALMERS
UNIVERSITY OF TECHNOLOGY

Department of Mechanics and Maritime Sciences
Division of Dynamics
CHALMERS UNIVERSITY OF TECHNOLOGY
Göteborg, Sweden 2020

Bandwidth Improvement of a Piezoelectric Micro Energy Harvester
JOHAN ANDERSSON

© JOHAN ANDERSSON, 2020

Master's thesis 2020:35
Department of Mechanics and Maritime Sciences
Division of Dynamics
Chalmers University of Technology
SE-412 96 Göteborg
Sweden
Telephone: +46 (0)31-772 1000

Cover:
Stress distribution on the surface of the energy harvester.

Chalmers Reproservice
Göteborg, Sweden 2020

Bandwidth Improvement of a Piezoelectric Micro Energy Harvester
Master's thesis in Applied mechanics
JOHAN ANDERSSON
Department of Mechanics and Maritime Sciences
Division of Dynamics
Chalmers University of Technology

ABSTRACT

Energy harvesting is a technology where electricity is generated from ambient energy resources. A piezoelectric energy harvester, which converts vibrations to electricity, is a promising power supply for sensors connected to the Internet of Things (IoT). This kind of power supply is self sustainable and does not need any maintenance nor external fuels.

The aim of this study is to propose a harvester design with large bandwidth for an IoT application on micro scale. The eigenfrequencies and frequency response of the harvester are predicted by finite element simulations and the simulation model is compared to experimental data. An electromechanical model (EMM) is compared to a simplified pure mechanical model (PMM) and a correlation is found between the two models. The frequencies are shifted by a factor 0.95, i.e. $f_{\text{EMM}}/f_{\text{PMM}} = 0.95$, and 1 mV corresponds to 7 MPa.

Key factors for bandwidth improvement are a small eigenfrequency gap and a high enough voltage level. The eigenfrequency gap is reduced with a back folded cantilever beam design with similar beam lengths and constant uniform thickness. For a given amplitude of the vibration source the total voltage output can be increased with a smaller coverage of piezoelectric material.

Improved bandwidth is shown for three different beam lengths. The tolerance from the centre frequency is about ± 1 %, which corresponds to a 114 Hz bandwidth in the 4100 Hz region.

Keywords: Energy harvesting, Piezoelectricity, MEMS, Bandwidth

PREFACE

This thesis is the final step to a Master of Science in Engineering. The work is based on studies in Engineering Physics and Applied Mechanics at Chalmers University of Technology during 2014-2020.

ACKNOWLEDGEMENTS

For the completion of this project I would like to express my gratitude to my supervisor Associate Prof. Peter Folkow. During the entire period I have got great support and important advice to help me proceed. When problems have occurred we have had constructive discussions to find new solutions. I would also like to thank Lic. of Engineering Agin Vyas for useful input on the fabrication process. Furthermore thanks to Associate Prof. Per Lundgren and Prof. Peter Enoksson for sharing your knowledge and experience in the field of electronics and micro energy harvesters.

Johan Andersson, June 2020

NOMENCLATURE

Abbreviations

COMSOL	A finite element simulation software
EMM	Electromechanical model
IoT	Internet of Things
MEMS	Microelectromechanical systems
PMM	Pure mechanical model
PZT	Lead zirconate titanate

List of symbols

A_i	Piezoelectric area on inner beam [m ²]
A_o	Piezoelectric area on outer beams [m ²]
b_f	Bandwidth [Hz]
\mathbf{C}	Damping matrix
d	Oscillation amplitude [m]
f	Frequency [Hz]
f_0	Eigenfrequency [Hz]
f_d	Damping frequency [Hz]
\mathbf{K}	Stiffness matrix
l_i	Inner beam length [m]
l_m	Outer proof mass length [m]
l'_m	Inner proof mass length [m]
l_o	Outer beam length [m]
\mathbf{M}	Mass matrix
t	Time [s]
t_b	Beam thickness [m]
t_m	Proof mass thickness [m]
t_p	PZT layer thickness [m]
U	Voltage [V]
\overline{U}	Surface average voltage [V]
w	Displacement [m]
w_g	Gap between inner and outer beam [m]
w_i	Inner beam width [m]
w_o	Outer beam width [m]
α	Mass damping coefficient [1/s]
β	Stiffness damping coefficient [s]
Δf	Eigenfrequency gap [Hz]
ζ	Damping ratio [-]
σ	Stress [Pa]
$\overline{\sigma}$	Surface average stress [Pa]
ω	Angular frequency [rad/s]

CONTENTS

Abstract	i
Preface	iii
Acknowledgements	iii
Nomenclature	v
Contents	vii
List of Figures	ix
List of Tables	ix
1 Introduction	1
1.1 Background	1
1.2 Aim	3
1.3 Limitations	3
2 Method	3
2.1 Geometry	3
2.2 Finite element analysis	4
2.2.1 Electromechanical model (EMM)	5
2.2.2 Pure mechanical model (PMM)	5
2.2.3 Damping	5
2.3 Simulation strategy	5
2.3.1 Computation of eigenfrequencies	5
2.3.2 Computation of frequency response	6
2.4 Post processing	6
3 Results	7
3.1 Model validation to experiments	7
3.2 Comparison of EMM and PMM	8
3.3 Eigenfrequency analysis	9
3.4 Voltage level	10
3.5 Bandwidth	13
4 Discussion	17
References	19

List of Figures

1.1	Schematic relation between voltage and frequency. If the eigenfrequencies are close to each other the inter peak valley rises.	2
1.2	A two degree of freedom cantilever design. The ends of the outer beams are attached to a fixture.	2
2.1	Sketch of harvester design with definition of design parameters. The structure is symmetric about the dashed line.	4
2.2	Side view of the outer beam and proof mass. The beam consists of two layers: PZT (dark) and silicon (light).	4
2.3	Mesh of the computational domain.	4
2.4	Definition of bandwidth. The dashed line indicates the threshold level of 100 mV and the bandwidth is the frequency range of which the voltage is higher than the threshold.	6
3.1	Voltage output from the EMM for different damping ratios, based on Shen et al. [15]	7
3.2	Ratio between voltage from the EMM and stress from the PMM.	8
3.3	Eigenfrequency gap as a function of beam length ratio.	9
3.4	Eigenfrequency gap as a function of proof mass thickness.	10
3.5	Electric potential distribution of one of the outer beams.	11
3.6	Mode shape with tension and compression on the surface of the outer beams. Deflection not to scale.	11
3.7	Voltage output from the outer beams. The beams are covered with piezoelectric material from the attachment boundary to a length with given ratio of the outer beam length l_o	12
3.8	Electric potential distribution of the inner beam.	12
3.9	Voltage output from the inner beam. The beam is covered with piezoelectric material from the outer proof mass boundary to a length with given ratio of the inner beam length l_i	13
3.10	Voltage output for $l_o = 2000 \mu\text{m}$	14
3.11	Voltage output for $l_o = 3000 \mu\text{m}$	15
3.12	Voltage output for $l_o = 4000 \mu\text{m}$	15
3.13	Voltage output for $l_o = 3000 \mu\text{m}$ and $t_m = 40 \mu\text{m}$	16
3.14	Voltage output for $l_o = 3000 \mu\text{m}$ and $l_i = 2900 \mu\text{m}$	17

List of Tables

3.1	Dimensions for the EMM and PMM comparison.	8
3.2	Design parameters for final design. All dimensions are in μm	13
3.3	Eigenfrequency gap, piezoelectric area coverage (absolute and relative), bandwidth and tolerance for the three studied cases of different beam lengths.	14

1 Introduction

The modern society requires electricity in order to work. In our digital era more and more units are connected to the so called Internet of Things (IoT). These units need electric supply, but some units cannot be connected to the mains. Furthermore these units often have sensors that are either small or located in areas which are hard to access. Batteries are not a suitable choice in that sense since they need maintenance, which can be either hard or even impossible. The electricity must be generated from some self sustainable device. An energy harvester is such a device. It generates electricity from ambient energy resources, such as vibrations, without any external fuels. The key idea is to let each IoT unit have its own small power plant, where the power plant is an energy harvester.

IoT applications with small sensors require energy harvesters on micro scale [1]. Electromagnetic harvesters, which are efficient for macro scale applications, cannot be easily scaled down. Miniaturisation of magnets and coils leads to fabrication issues as well as significantly decrease in efficiency. The piezoelectric energy harvester is more suitable and beneficial for micro scale applications [2].

This thesis work investigates the opportunity to harvest energy on micro scale. The study is developed from previous work made by Vyas [3] and Staaf [4].

1.1 Background

A piezoelectric material is a material that generates electricity from mechanical stress. The effect is due to the crystalline structure of the material. When a stress is applied the piezoelectric material gets polarised and an electrical charge is induced [5]. Lead zirconate titanate (PZT) is one of the best materials with respect to high piezoelectric properties. Furthermore PZT is flexible and ductile, which means that it has a good mechanical workability. These properties make PZT a suitable material for piezoelectric energy harvesters in general, and for micro scale devices in particular [6].

The output from a piezoelectric energy harvester is maximised at its resonance frequency, even called eigenfrequency. Therefore every harvester must be designed with an eigenfrequency that coincides with the frequency range for a particular application. One of the most challenging issues is the significant output decrease when the vibrational frequency slightly shifts. The narrow bandwidth makes the harvester inefficient since most applications have some frequency variation [7].

One way to increase the bandwidth, i.e. harvestable frequencies, is to attach several single cantilevers to the vibration source in an array. The cantilevers should have eigenfrequencies that are slightly shifted from each other in order to cover the operating frequency spectrum. Even though each cantilever has a narrow bandwidth their overlap result in a total wide bandwidth [8]. However, for this solution only one cantilever generates electricity at a time which makes the design inefficient. Furthermore another disadvantage is that the design requires much space if the harvester is to cover a wide range of frequencies, since that requires many cantilevers [4].

Another way to increase the bandwidth is to make a design such that the eigenfrequencies are close to each other. If the eigenfrequency gap, Δf , is small enough the inter peak valley rises according to Figure 1.1. Hence the range of continuous frequencies with high voltage increases as the inter peak valley rises, i.e. the bandwidth increases [4]. The eigenfrequency gap can easily be reduced with a two degree of freedom cantilever design, which consists of two main beams and one secondary beam [9]. The design is shown in Figure 1.2. The outer, main beams, are attached to a fixture which is subjected to vibrations. A proof mass is put at the connection link between the beams and at the end of the inner, secondary beam. This two degree of freedom design generates a higher total output and a wider bandwidth than the array of equivalent single degree of freedom cantilevers [10]. Furthermore the backfolded design enables the energy harvester to be small and area efficient. This planar design is possible and desirable for fabrication on micro scale [4].

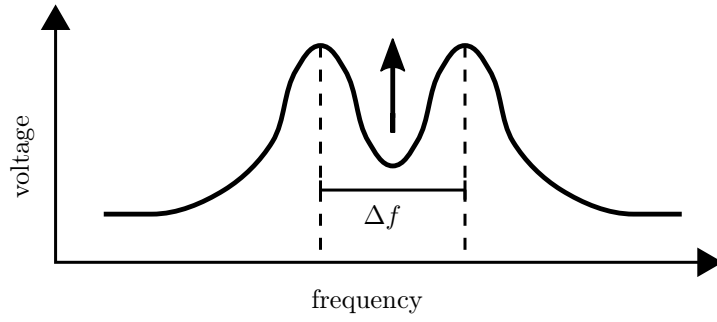


Figure 1.1: Schematic relation between voltage and frequency. If the eigenfrequencies are close to each other the inter peak valley rises.

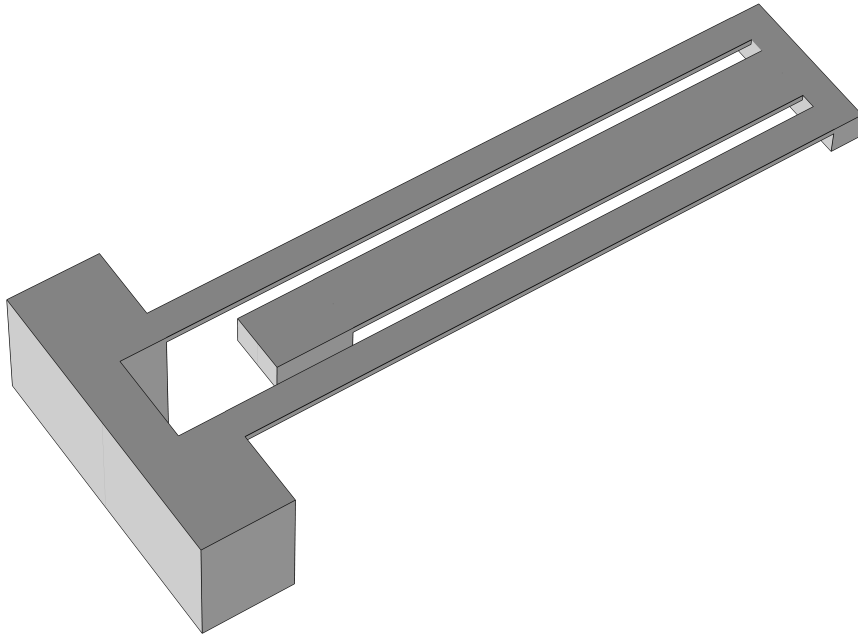


Figure 1.2: A two degree of freedom cantilever design. The ends of the outer beams are attached to a fixture.

1.2 Aim

The aim of this thesis is to develop a functional design for a piezoelectric energy harvester on micro scale for an IoT application. A design is considered functional if the harvester generates a significant voltage for a large range of frequencies. The design development starts from a backfolded two degree of freedom design, which is promising with respect to bandwidth improvement. Results from this study will contribute to future fabrication of functional piezoelectric energy harvesters on micro scale.

The design development is divided into several tasks. Two proposed simulation models are investigated for the electromechanical analysis of the device. These models include assumptions which the rest of the development are based on. Furthermore design parameters of the device, such as length and thickness, are related to eigenfrequencies, eigenfrequency gap and voltage output. Finally the main task is to propose a design that is promising with respect to large bandwidth.

1.3 Limitations

This study is limited to cover geometric and electromechanical analysis of the energy harvester. The two studied models are an electromechanical model (EMM) and a pure mechanical model (PMM), and the harvester is simplified to only include two materials; silicon and PZT. Furthermore the vibration source is simplified to harmonic motion with constant amplitude. The behaviour of the energy harvester is predicted by simulations in COMSOL Multiphysics 5.5. Since fabrication of microelectromechanical systems (MEMS) are hard and time consuming it is considered to be outside the scope of this thesis. Nevertheless all dimensions of the device are subjected to fabrication ability.

2 Method

The start point of the design development was a study by Vyas et al. [1]. From that study the proposed design was promising with respect to small eigenfrequency gap and fabrication ability. In the following sections the geometry of the design is defined and the assumptions of the finite element analysis, together with boundary conditions, are stated. Furthermore it is followed by a brief description of the simulation strategy and the post processing.

2.1 Geometry

The key design concept of this study was a backfolded and in plane two degree of freedom structure. The structure consists of two outer and one inner cantilever beam, as well as one outer and inner proof mass. The outer beams are clamped to a fixture which is subjected to vibrations from its surroundings. A sketch of the design is presented in Figure 2.1. In the figure the proof masses are indicated by the light areas.

In the study by Vyas et al. the fabrication process of a piezoelectric micro energy harvester is described. The beams consisted of several thin layers of different materials. These were, from top to bottom, 100 nm platinum, 20 nm titanium, 1 μm PZT, 100 nm LaNiO, another 100 nm and 20 nm of platinum and titanium, 500 nm silicon dioxide and finally 20 μm silicon. The proof masses were made of a 500 nm silicon dioxide layer and the rest was silicon [1]. The choice of materials was simplified into two models for this study, where the simplification was based on materials with significant layer thickness, i.e. silicon and PZT. For the first model the cantilever beams were simplified to a two layered material model. One layer of silicon and one layer of PZT, where the PZT thickness t_p was set to 1 μm . Both proof masses were considered one layer of silicon. In the second model the entire structure was considered to be made of silicon. A layer overview with parameter definitions is presented in Figure 2.2.

Due to fabrication abilities the thicknesses of the cantilever beams must be equal and constant, i.e. no spatial variations. Fabrication of the beams were constrained to 20 μm thickness at the time of this study ($t_b = 20 \mu\text{m}$) [11]. Similarly the proof masses must have equal and constant thicknesses, but it may differ from the cantilever beam thickness. In order to guarantee free motion of the cantilever beams the distance between the beams, w_g , must be at least 50 μm . Finally the smallest in plane feature size is 5 μm [12].

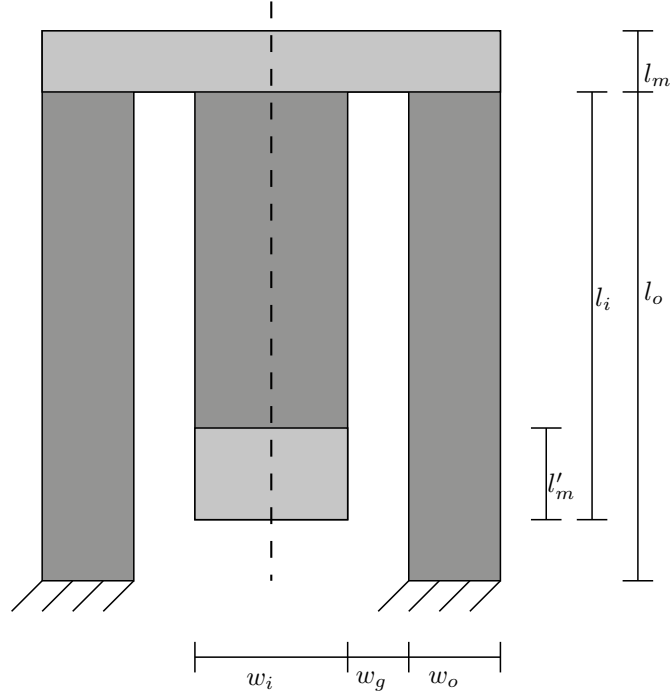


Figure 2.1: Sketch of harvester design with definition of design parameters. The structure is symmetric about the dashed line.

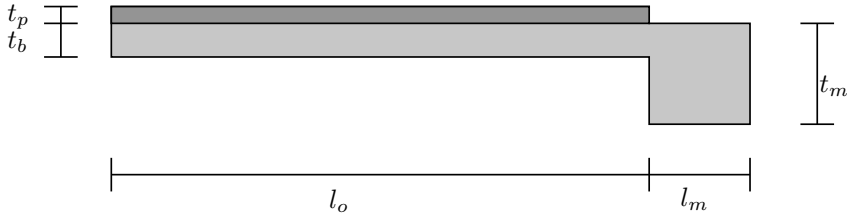


Figure 2.2: Side view of the outer beam and proof mass. The beam consists of two layers: PZT (dark) and silicon (light).

2.2 Finite element analysis

The finite element analysis was carried out with COMSOL Multiphysics 5.5. Since the structure is very thin with respect to its length, the structure was treated as a shell. Two dimensional shell elements were used for the computation which reduced the total degrees of freedom to be solved for. Due to symmetry in the geometry only half the structure was considered during the simulations. Figure 2.3 shows the meshed computation domain. The edge of the outer beam had a prescribed harmonic out of plane motion with no rotation. Since the device can be orientated on the vibration source in a way such that pure out of plane motion is obtained,

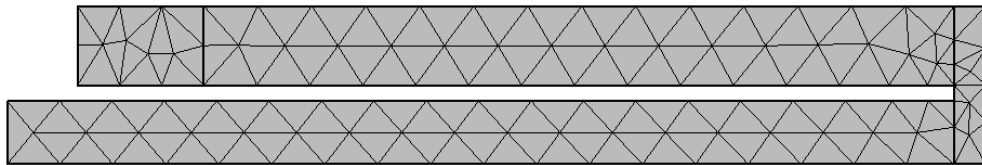


Figure 2.3: Mesh of the computational domain.

this assumption was made without loss of generality. The prescribed displacement w was defined by a given amplitude d and angular frequency $\omega = 2\pi f$ according to

$$w(t) = d \sin \omega t. \quad (2.1)$$

Two different types of analyses were performed for the simplified model presented in section 2.1. For the first model a piezoelectric electromechanical analysis was performed and a pure mechanical analysis was performed for the second model.

2.2.1 Electromechanical model (EMM)

In this model the structure was considered as a layered shell. The silicon layer was set to be linear elastic and the PZT layer was set to be piezoelectric. The four parts, inner and outer beams and proof masses, were connected with a continuity boundary condition. Electric insulation enclosed the beams and no electric currents were allowed in the silicon proof masses. The interface between the silicon and PZT in the beams was set to ground potential.

2.2.2 Pure mechanical model (PMM)

In the PMM the entire structure was made of silicon. The material was considered to be linear elastic. For comparisons with the electromechanical model the total thickness of the beams was equal for both models, i.e. the PZT layer from the electromechanical model is replaced by silicon of the same thickness.

2.2.3 Damping

Mechanical damping was added for the linear elastic and piezoelectric materials for both models. Rayleigh damping was used for this study, where the damping matrix \mathbf{C} is a linear combination of the mass and stiffness matrices of the system, \mathbf{M} and \mathbf{K}

$$\mathbf{C} = \alpha \mathbf{M} + \beta \mathbf{K}. \quad (2.2)$$

Here α and β are given by

$$\alpha = 4\pi f_{d1} f_{d2} \frac{\zeta_1 f_{d2} - \zeta_2 f_{d1}}{f_{d2}^2 - f_{d1}^2}, \quad (2.3)$$

$$\beta = \frac{\zeta_2 f_{d2} - \zeta_1 f_{d1}}{\pi(f_{d2}^2 - f_{d1}^2)}, \quad (2.4)$$

where ζ_i is the damping ratio at frequency f_{di} [13]. The damping frequencies were chosen to be the same as the first and second eigenfrequency, since damping is necessary where the response is large. The choice of damping model was not further investigated and for this study the damping ratios ζ_1 and ζ_2 were assumed to be equal.

2.3 Simulation strategy

The simulations were divided into two subtasks. The first subtask was to find the first and second eigenfrequency of the structure. When the eigenfrequencies were determined the following subtask was to compute the frequency response for a frequency range including the eigenfrequencies. These two subtasks were connected to the following problems: get the eigenfrequencies close enough and the voltage output high enough.

2.3.1 Computation of eigenfrequencies

The first two eigenfrequencies, f_{01} and f_{02} , were computed with the eigenfrequency solver in COMSOL. Different design parameters, such as width, length and thickness of the beams and proof masses, were varied with a parametric sweep. With this strategy the eigenfrequencies were computed for several designs in one single run. The eigenfrequency gap $\Delta f = f_{02} - f_{01}$ was computed for each set of design parameters. A design was considered useful if Δf was less than 5 % of the centre frequency, average of first and second eigenfrequency.

2.3.2 Computation of frequency response

The determination of eigenfrequencies was followed by a frequency response study. In this step the frequency of the prescribed motion in (2.1) was varied, and the response was solved for the stationary solution for each frequency. The frequency range was chosen such that both eigenfrequencies were covered, with an additional span of 2 % on each side.

2.4 Post processing

Post processing of the simulation results was divided into two parts. Extraction of quantities of interest from the computed solution and data handling. The extraction part was carried out in the COMSOL results interface and MATLAB 2018b was used for the other part.

For the EMM the voltage on the top of the PZT layer was computed. In order to get voltage as a function of frequency a surface average was calculated to be the actual output. To avoid cancellation effects as the inner and outer beams might vibrate with shifted phase, the beams were treated as two separate systems. Hence the total voltage output was the sum of the absolute values from each contribution.

$$U = |\bar{U}_{\text{in}}| + 2|\bar{U}_{\text{out}}| \quad (2.5)$$

Similarly the beams were treated as two separate systems for the PMM. Instead of voltage a surface average of the stress was computed on the top of the silicon beams. Since the motion of the structure ideally was pure out of plane, the stress tensor had the major contribution from the component which coincided with the length of the structure. The output measure was simplified to only regard that component, which also allowed distinction between compression and tension for the surface average calculation.

$$\sigma = |\bar{\sigma}_{\text{in}}| + 2|\bar{\sigma}_{\text{out}}| \quad (2.6)$$

In order to compare the output from different designs the bandwidth b_f was introduced as the measure of interest. This measure was related to a threshold level of 100 mV, which is the required useful voltage for electric circuits in micro scale. Voltages above this threshold was considered to be harvestable [14]. An illustration of the bandwidth is presented in Figure 2.4. A design with larger bandwidth was considered better, regardless of peak voltage or inter peak valley voltage.

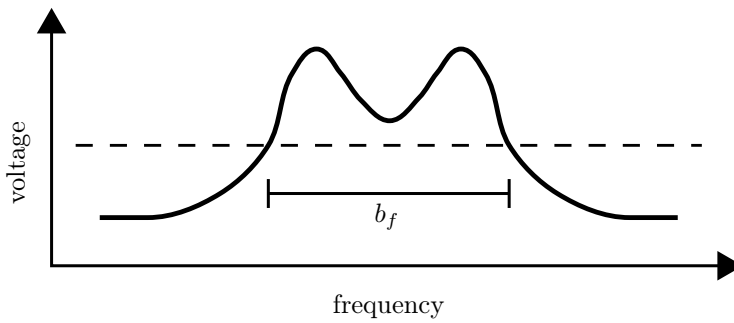


Figure 2.4: Definition of bandwidth. The dashed line indicates the threshold level of 100 mV and the bandwidth is the frequency range of which the voltage is higher than the threshold.

3 Results

The presentation of the results is divided into several parts. Firstly there are two sections about reliability of the simulation models. The following two sections are about design strategies that make an effective energy harvester. In the final section the previous results are used to propose an energy harvester design with improved bandwidth.

Three types of COMSOL simulation models were used: 3D solid, multilayered shell and single layered shell. The 3D solid and multilayered shell models simulated the EMM with silicon and PZT. Three dimensional tetrahedral elements were used in the solid model and two dimensional triangular elements were used in the shell model. The latter element type was also used in the single layered shell simulation model, but the only material was silicon according to the PMM. All three models gave similar results but the 3D solid model had a 100 times longer computation time due to more elements. The multilayered shell model is a special feature in COMSOL which only was available for a limited time during this project. Most results in this study was therefore computed with the single layered shell model.

All simulations included a mesh size study. The aim of that study was to check convergence of eigenfrequencies and voltage/stress, in order to guarantee that an appropriate mesh size was used.

3.1 Model validation to experiments

Experiments have been performed on a single cantilever beam made of silicon and PZT by Shen et al. [15]. The device was on micro scale with similar geometric dimensions and materials as the energy harvester in the scope of this thesis. In order to validate the relevance of the assumptions in the EMM, the experimental results were reproduced by COMSOL simulations of the EMM. The oscillation amplitude d was set to $0.12\text{ }\mu\text{m}$, which corresponds to an acceleration of 1.0 g . The eigenfrequency from the simulations was 468 Hz , while 461 Hz was the measured eigenfrequency from the experiments. In Figure 3.1 the voltage output from the EMM is presented for some damping ratios ζ used in the study by Shen et al. From the figure it is clear that the peak value is strongly dependent of the choice of damping ratio. However the order of magnitude of the voltage

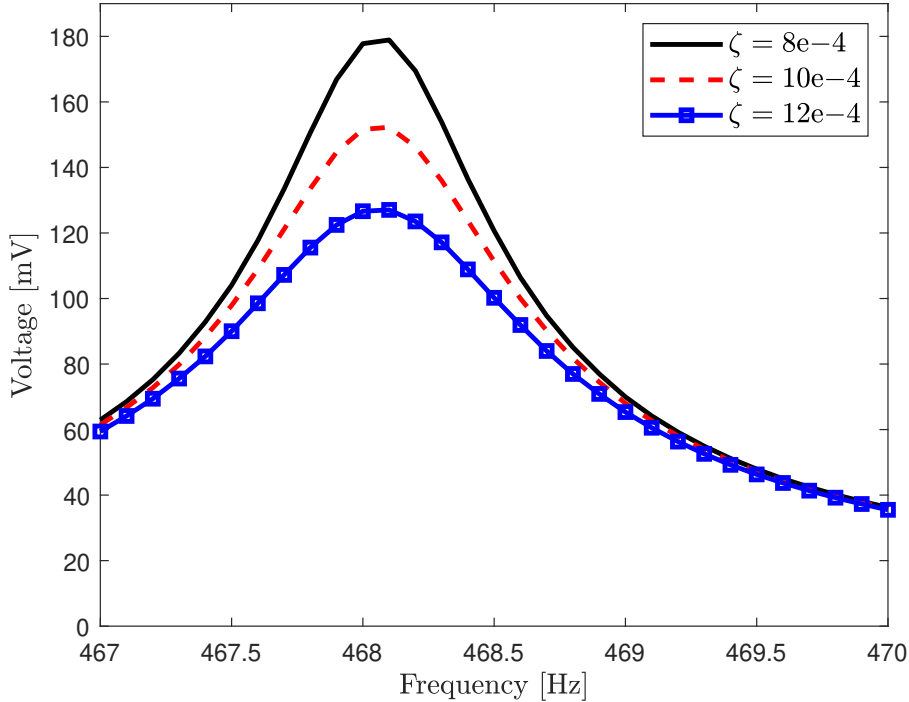


Figure 3.1: Voltage output from the EMM for different damping ratios, based on Shen et al. [15]

output from the simulations is similar to the measured data from the experiments by Shen et al. [15]. Based on these experimental data, the oscillation amplitude and damping ratio in the following simulations were set to $d = 0.12 \mu\text{m}$ and $\zeta = 10^{-3}$.

3.2 Comparison of EMM and PMM

Simulations were run for the EMM and PMM with the same geometry. The geometries that were studied were different beam thicknesses, lengths of the outer beam and thicknesses of the proof masses. All combinations of the dimensions presented in Table 3.1 were used, which resulted in a total of 175 different designs. The restriction of $t_b = 20 \mu\text{m}$ was unknown when these simulations were run, which is the reason why variations of t_b are included. In an early stage of this project a beam length ratio of 0.98 was found to be beneficial with respect to eigenfrequency gap reduction. Due to that the length of the inner beam was 98 % of the outer beam length in this comparison. Furthermore the impact of proof mass thickness to eigenfrequency gap was not yet investigated, which motivates why t_m in this model comparison was chosen differently to the final thickness in section 3.5. A more thorough investigation of Δf is presented in section 3.3. Except for the parameters in Table 3.1 and the inner beam length l_i , all other design parameters were constant for this comparison.

Table 3.1: Dimensions for the EMM and PMM comparison.

$t_b + t_p$ [μm]	21, 26, 31, 36, 41
l_o [μm]	2500, 2750, 3000, 3250, 3500, 3750, 4000
t_m [μm]	50, 62.5, 75, 87.5, 100

The eigenfrequencies were shifted between the models. However, the quotient $f_{0\text{EMM}}/f_{0\text{PMM}}$ was approximately 0.95 for both the first and second eigenfrequency for all designs. Further on the start and stop frequencies of the frequency response analysis was related to the eigenfrequencies of each model. There were 61 frequencies in the range of analysis for all designs and models. Figure 3.2 shows the relation between the EMM voltage and the PMM stress for each frequency. Each frequency has 175 points which correspond to the different designs. The relation is most uncertain at the eigenfrequencies and there is less variation for the other frequencies. An

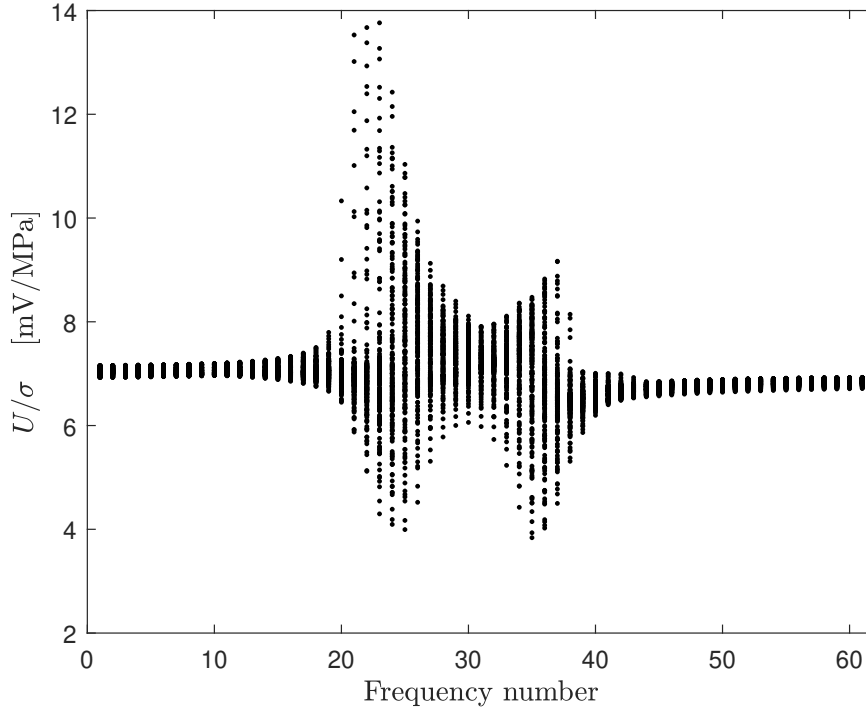


Figure 3.2: Ratio between voltage from the EMM and stress from the PMM.

average of the quotients results in a conversion factor of 7 mV/MPa, with an average error of 13 %.

Based on these results the following simulations were simplified to only use the PMM. The voltage was approximated by the stress according to

$$U = 7 \cdot 10^{-9} \sigma \quad (3.1)$$

and the frequencies were shifted by a factor of 0.95.

3.3 Eigenfrequency analysis

The eigenfrequencies of the energy harvester were computed according to section 2.3.1. It was found that the length of the beams had the most significant impact on the eigenfrequencies. Longer beams resulted in lower eigenfrequencies and vice versa. The gap between the first two eigenfrequencies was strongly dependent on the ratio between the lengths of the inner and outer beams, l_i/l_o . Figure 3.3 shows how the eigenfrequency gap changes for varying beam length ratios for three different beam lengths. The eigenfrequency gap was minimised when the beams had approximately equal length. Furthermore Δf was increased when the proof mass thickness t_m was increased. Since t_b is restricted to 20 μm an equal thickness of beam and proof mass sections was the best configuration with respect to minimising Δf , which is shown in Figure 3.4. Finally it was found that a small gap width, w_g , between the beams was beneficial with respect to small Δf .

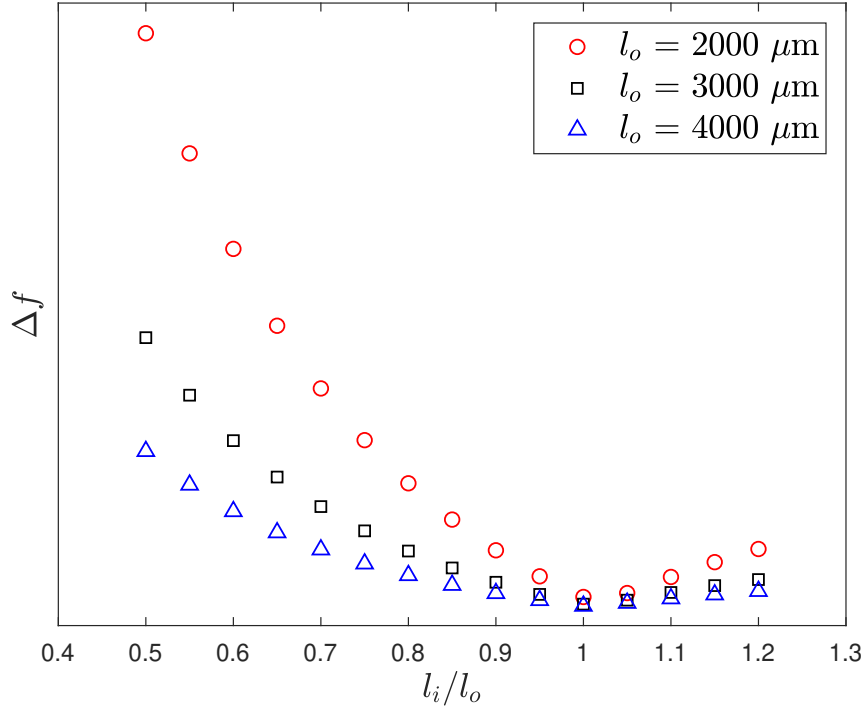


Figure 3.3: Eigenfrequency gap as a function of beam length ratio.

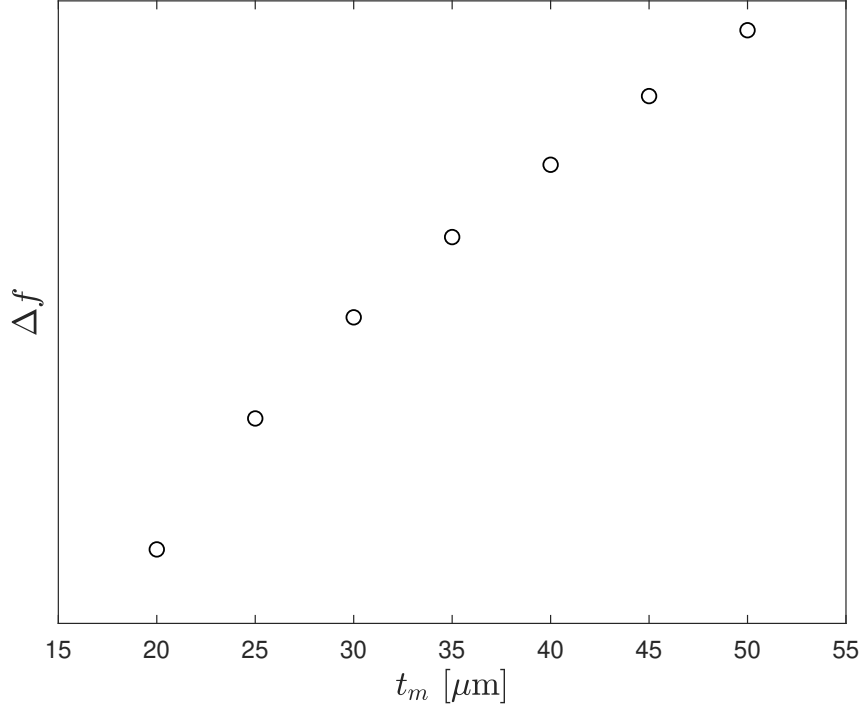


Figure 3.4: Eigenfrequency gap as a function of proof mass thickness.

3.4 Voltage level

Factors that affect the voltage level were investigated in order to meet the requirements of bandwidth, stated in section 2.4. The choice of damping ratio has a big impact, which is shown in section 3.1. Furthermore larger oscillation amplitudes results in increasing voltages. However, since the determination of damping ratio is uncertain without experimental measurements and the oscillation amplitude is application dependent, those factors were set constant for the voltage level investigation.

Results from section 3.2 suggests a relation between stress and induced voltage. Due to geometry and motion of the device, the stress varies along the length of the beam, while stress variations across the beam width are considered negligible. The corresponding electric potential distribution along the length of the outer beam is presented in Figure 3.5. The eigenfrequencies of the considered structure were 1773 Hz and 1816 Hz. For frequencies below the first eigenfrequency there was pure tension (or compression) and for higher frequencies there was a mix of tension and compression along the beam. An example of the mode shape with mixed tension and compression is shown in Figure 3.6. The useful output voltage from an electrode is the average potential from the entire beam surface. Thus a mixture of tension and compression on the same beam is not desirable, since some contributions to the total output is cancelled out for that particular frequency. Consequently the total voltage depends on how much of the beam that is covered with piezoelectric material. However the information of the potential distribution in Figure 3.5 does not tell anything about the relation between piezoelectric coverage and output, since the potential changes sign at different beam lengths for each particular frequency. For some frequencies the major output contribution comes from the attached end of the beam and for other frequencies the major contribution comes from the proof mass end of the beam. Different piezoelectric coverage ratios were investigated and Figure 3.7 shows the frequency response. The voltage decreases for increasing piezoelectric coverage. However, smaller coverage implies less generated current and thus less power. Therefore it would be desirable to go for a large piezoelectric coverage, but still reach a significant voltage level with respect to a threshold of 100 mV.

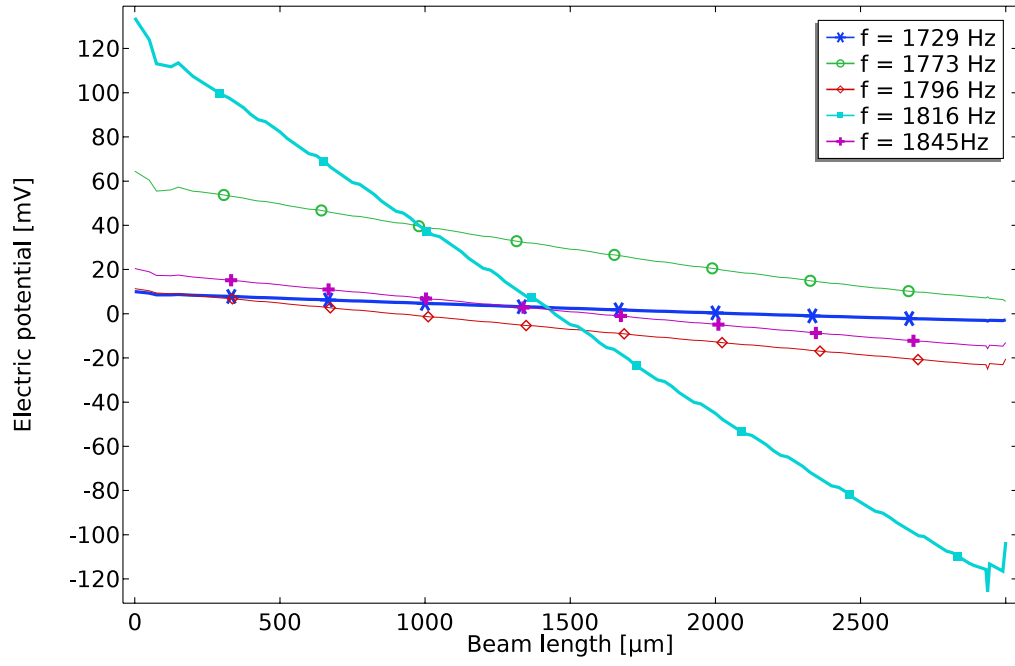


Figure 3.5: Electric potential distribution of one of the outer beams.

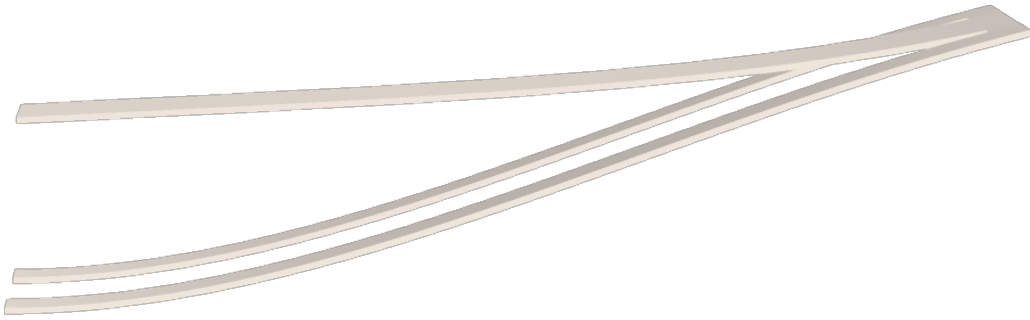


Figure 3.6: Mode shape with tension and compression on the surface of the outer beams. Deflection not to scale.

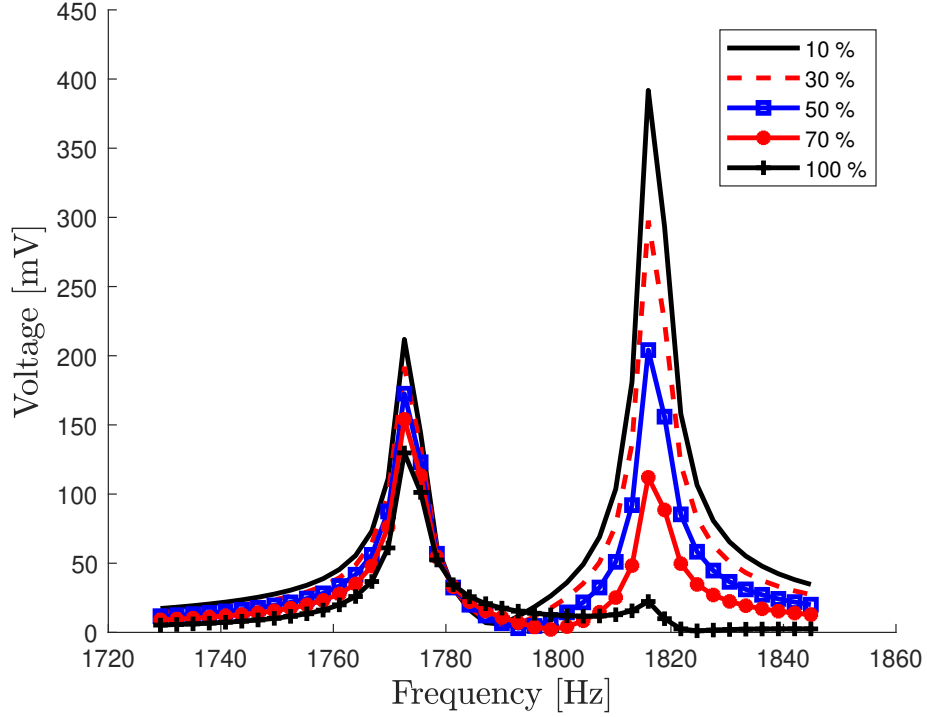


Figure 3.7: Voltage output from the outer beams. The beams are covered with piezoelectric material from the attachment boundary to a length with given ratio of the outer beam length l_o .

Similarly the electric potential distribution for the inner beam is presented in Figure 3.8. On the contrary to the outer beam, the inner beam has pure tension (or compression) along its entire beam length. The beam length is measured from the outer proof mass. The frequency response for the inner beam is shown in Figure 3.9. In comparison to the outer beams the inner beam generates a lower voltage. Furthermore the inner beam is not as effective at both eigenfrequencies as the outer beams.

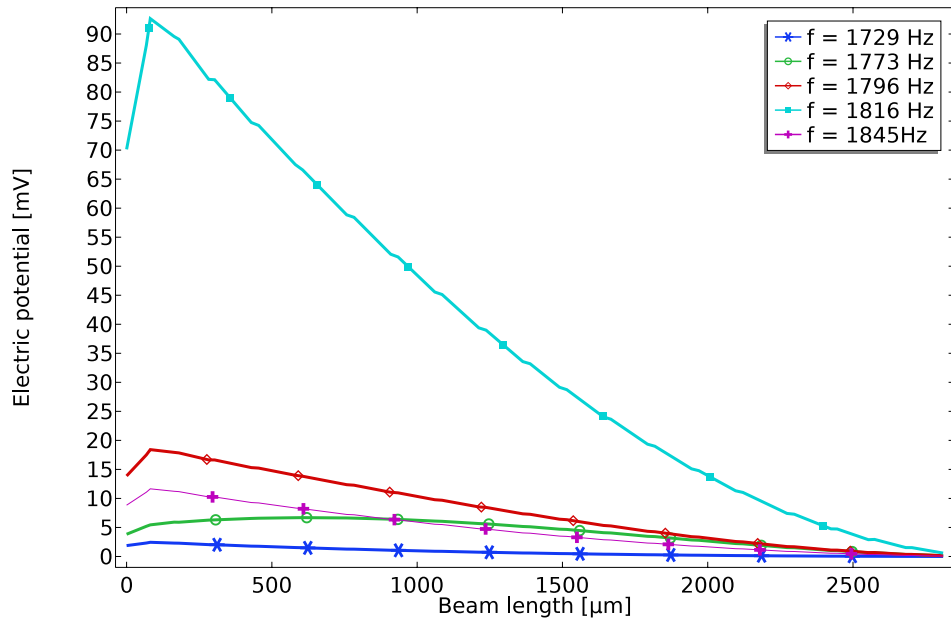


Figure 3.8: Electric potential distribution of the inner beam.

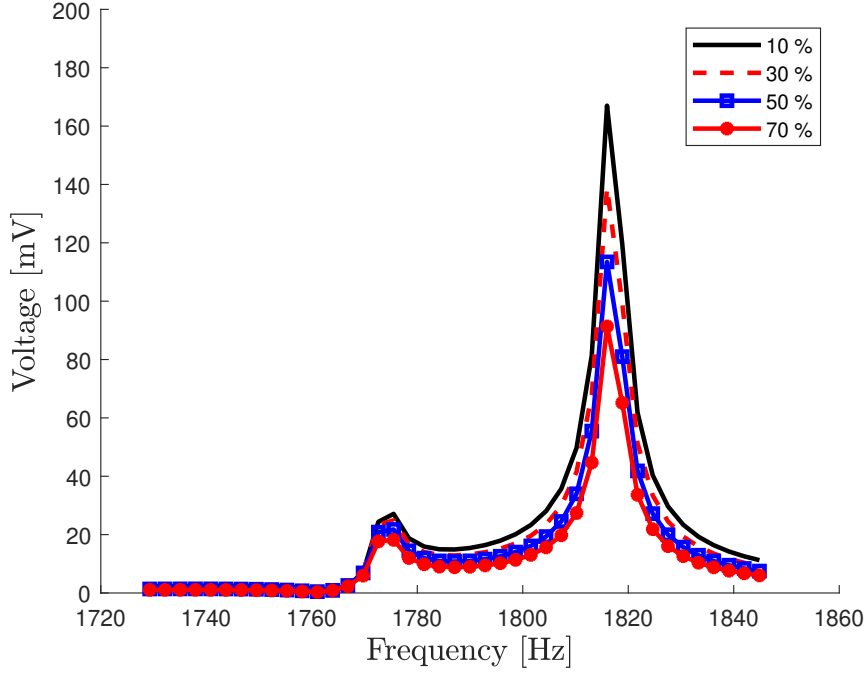


Figure 3.9: Voltage output from the inner beam. The beam is covered with piezoelectric material from the outer proof mass boundary to a length with given ratio of the inner beam length l_i .

3.5 Bandwidth

The development of a design proposal with respect to large bandwidth was based on the results from the eigenfrequency analysis in section 3.3 and the voltage level analysis in section 3.4. The bandwidth problem was a combination of these two parts. Firstly, in order to get the interaction effect from the two eigenfrequency peaks, the eigenfrequency gap Δf had to be small enough. Furthermore the voltage level had to be high enough to reach above the threshold level. Since no experiments were performed in this study the oscillation amplitude and damping ratio was chosen according to the validation in section 3.1, i.e. $d = 0.12 \mu\text{m}$ and $\zeta_i = 10^{-3}$.

The solution of the eigenfrequency part was achieved with equal beam and proof mass thickness, smallest allowed beam gap width and similar beam lengths. All parameters that were constant throughout the simulations are presented in Table 3.2. Since the entire structure was chosen to have the same thickness, t_p of $1 \mu\text{m}$ was neglected for simplicity. With the same reason the inner proof mass length l'_m had no importance for this geometry.

Table 3.2: Design parameters for final design. All dimensions are in μm .

t_b	20
t_m	20
w_g	50
w_o	200
w_i	400
l_m	100

Simulations were run for three different beam lengths, in order to investigate three different frequency areas. For each case the inner beam length was adjusted to reduce Δf . The voltage output for these three cases are shown in Figure 3.10, 3.11 and 3.12. All figures show the contribution from the inner beam and the two outer beams, as well as the total output. The green dotted line indicates the threshold level of 100 mV. In order to get an output above the threshold the piezoelectric coverage was changed according to section 3.4.

Since a larger piezoelectric area generates a higher current, and thus higher power, it was desirable to have as large piezoelectric area as possible. The results from the three studied cases, including eigenfrequency gap, piezoelectric area and bandwidth, are summarised in Table 3.3. The tolerance is the maximum deviation from a design frequency which ensures a harvestable output.

Table 3.3: Eigenfrequency gap, piezoelectric area coverage (absolute and relative), bandwidth and tolerance for the three studied cases of different beam lengths.

l_o [μm]	l_i [μm]	Δf [Hz]	A_o [mm^2]	A_i [mm^2]	A_o [%]	A_i [%]	b_f [Hz]	tolerance [%]
2000	2000	79	0.80	0.32	100	40	114	± 1.4
3000	2990	16	1.20	0.36	100	30	23	± 0.6
4000	3980	5	1.12	0.16	70	10	8	± 0.4

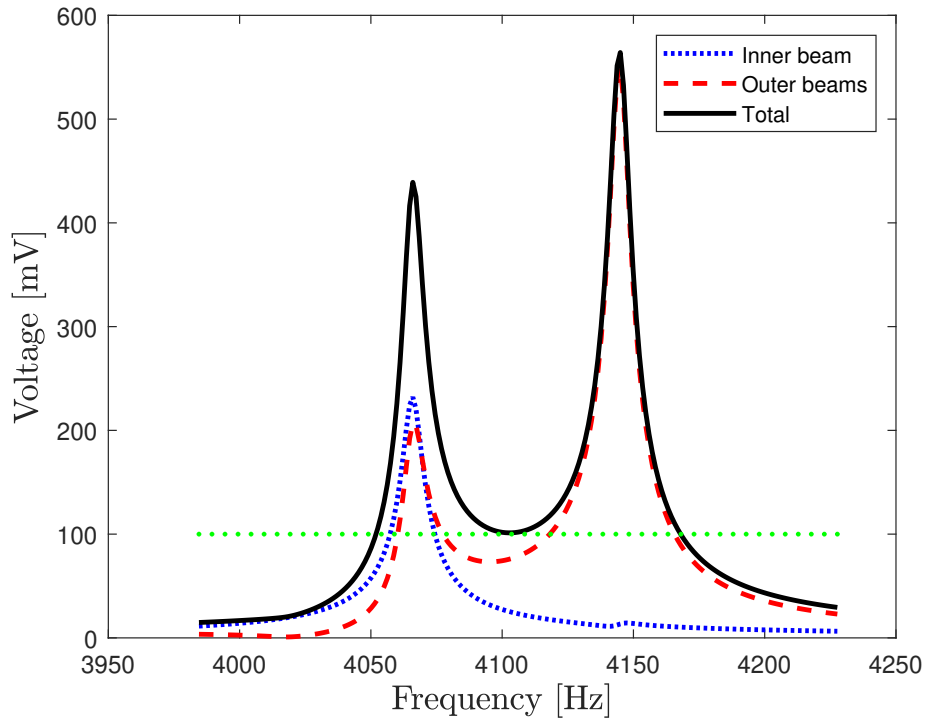


Figure 3.10: Voltage output for $l_o = 2000 \mu\text{m}$.

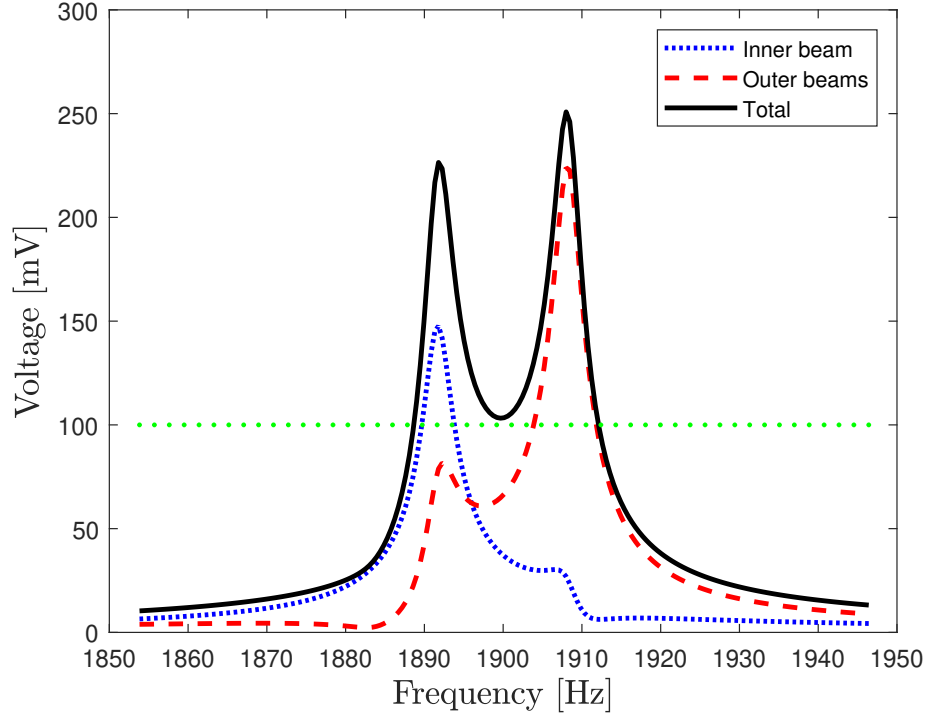


Figure 3.11: Voltage output for $l_o = 3000 \mu\text{m}$.

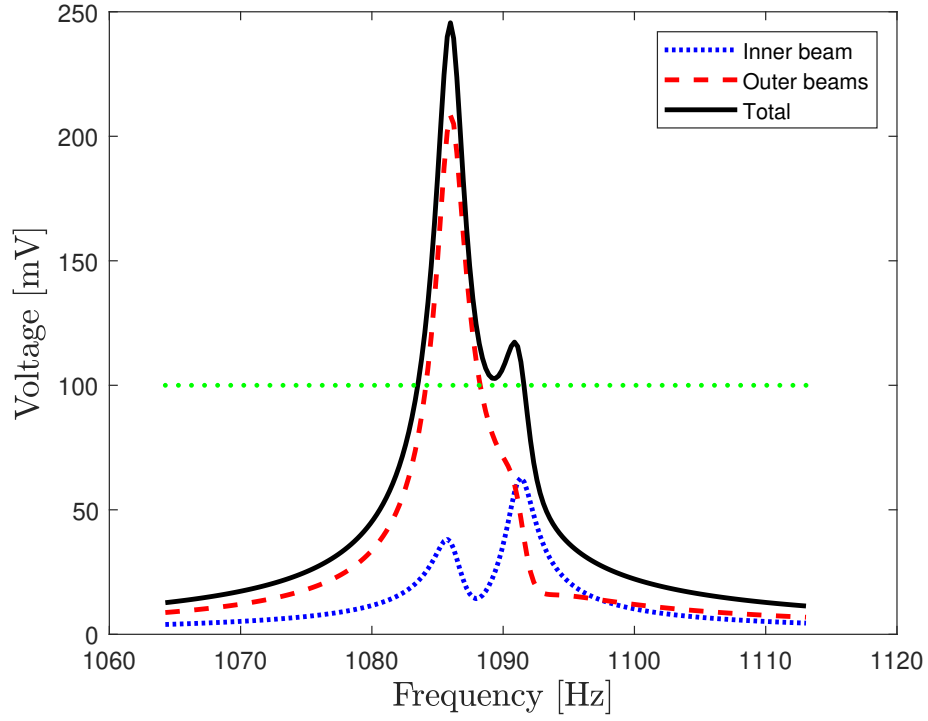


Figure 3.12: Voltage output for $l_o = 4000 \mu\text{m}$.

In order to illustrate the effects from the beam length ratio and the proof mass thickness on the final output, non optimal values with respect to reducing Δf were chosen for the 3000 μm design. In the first case t_m was set to 40 μm and in the second case $l_i = 2900 \mu\text{m}$. The same piezoelectric coverage was used as for the proposed design, i.e. 100 % for the outer beams and 30 % for the inner beam. The results are presented in Figure 3.13 and Figure 3.14. The voltage level is similar to the proposed 3000 μm design in Figure 3.11 around the eigenfrequencies, but much lower in the inter peak area. There is no rising inter peak valley effect for these non optimal choices of t_m and l_i , and consequently no significant bandwidth improvement. This illustrates the importance of a small Δf .

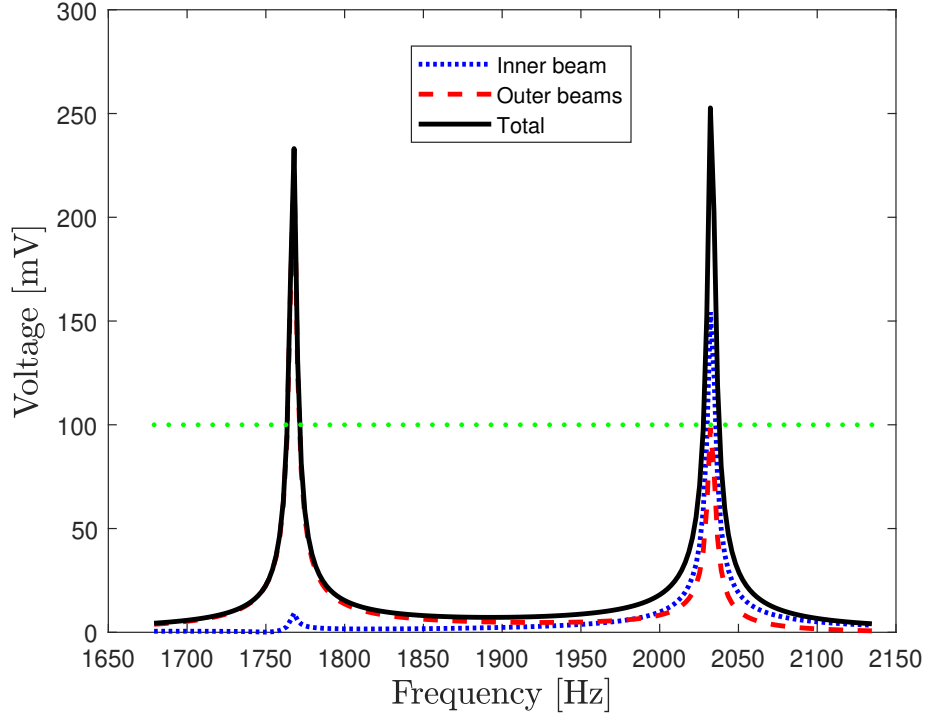


Figure 3.13: Voltage output for $l_o = 3000 \mu\text{m}$ and $t_m = 40 \mu\text{m}$.

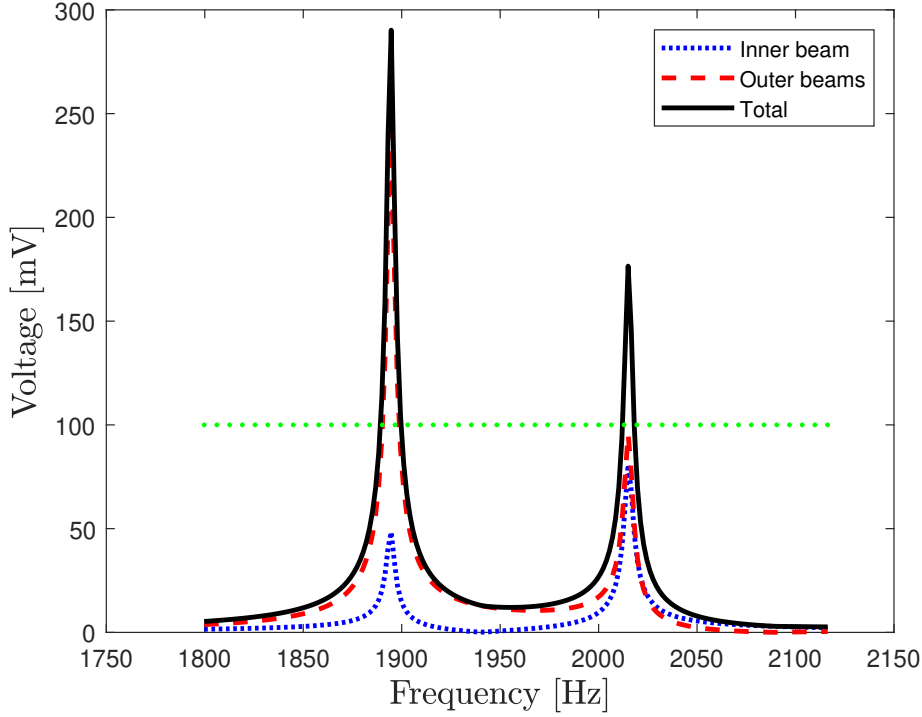


Figure 3.14: Voltage output for $l_o = 3000 \mu\text{m}$ and $l_i = 2900 \mu\text{m}$.

4 Discussion

The results from the simulated EMM are shown to be similar to the the experimental results by Shen et al. for a single cantilever piezoelectric micro energy harvester [15]. With the same materials, silicon and PZT, in the present work it is most likely that the EMM will be a good match to future experiments for the behaviour of a two degree of freedom design as well. Results from the simulations will be realistic in the sense of order of magnitude. The comparison between the EMM and PMM shows that there is a correlation between stress and voltage. This correlation motivates why the simplification of mechanical analysis is valid to predict the output voltage. However, there are uncertainties in the choice of damping model and oscillation amplitude which have a significant impact on the final output. Furthermore the damping may also be oscillation amplitude dependent.

The eigenfrequency gap, Δf , is shown from the frequency response analysis to have big impact on the bandwidth. Δf has to be rather small in order to get a rising inter peak valley effect. Similar beam lengths and uniform constant thickness of the device are promising factors in order to reduce Δf , which is the major contribution from this project to future work. The peak voltage level is lower in the low frequency region which makes it harder to find a design with output above the threshold. This can be solved with reduced PZT coverage, with a reduced power output as an assumed drawback. For the three studied designs the relative bandwidths are similar with a tolerance of about $\pm 1 \%$. Since each design is application dependent and works for different frequencies, no design is considered better with respect to bandwidth. However, all the three proposed designs show an improvement of bandwidth for three different frequency areas.

A drawback with the PMM is that nothing is told about the electric power. The simulation model must in some way include electricity and a circuit connection. There is probably a trade off between the voltage and power output, which is related to the PZT coverage on the beams. That would be the next thing to investigate.

In order to make any further conclusions, experimental measurements on a fabricated harvester are necessary. The results from this study can predict promising candidates for a given vibration application (frequency and amplitude), but the simulation model is too uncertain to give precise quantitative results. The most crucial part is application dependent damping model. A suggestion for future work is to fabricate a pure silicon device and measure the deflection in operation. This fabrication is much faster and cheaper than fabrication of the

full electronic device. However the mechanical properties are still similar, which implies reliable measurements for the damping model calibration.

Another thing that may be interesting to investigate is an attachment of the inner beam instead of the outer beams. This two degree of freedom device may remain the effect of closing the first two eigenfrequencies, but maybe result in other stress distributions than the ones presented in this study.

References

- [1] A. Vyas et al. A Micromachined Coupled-Cantilever for Piezoelectric Energy Harvesters. *Micromachines* **9**.252 (2018). DOI: 10.3390/mi9050252.
- [2] K. Tao et al. “Micro electret-based power generator for ambient vibrational energy harvesting”. *Energy harvesting: Technology, methods and applications*. Nova Science Publishers, 2016, pp. 23–24.
- [3] A. Vyas. “Towards an on-chip power supply”. Licentiate thesis. Chalmers University of Technology, 2019.
- [4] H. Staaf. “Conjoined piezoelectric harvesters and carbon supercapacitors for powering intelligent wireless sensors”. PhD thesis. Chalmers University of Technology, 2018.
- [5] J. A. Gallego-Juarez. Piezoelectric ceramics and ultrasonic transducers. *Journal of Physics E: Scientific Instruments* **22**.10 (1989), 804–816. DOI: 10.1088/0022-3735/22/10/001.
- [6] M. Kimura, A. Ando, and Y. Sakabe. “Lead zirconate titanate-based piezo-ceramics”. *Advanced piezoelectric materials*. Woodhead publishing limited, 2010, pp. 89–110.
- [7] L. Tang, Y. Yang, and C. Soh. Toward Broadband Vibration-based Energy Harvesting. *Journal of Intelligent Material Systems and Structures - J INTEL MAT SYST STRUCT* **21** (2010), 1867–1897. DOI: 10.1177/1045389X10390249.
- [8] H. Xue, Y. Hu, and Q. Wang. Broadband piezoelectric energy harvesting devices using multiple bimorphs with different operating frequencies. *IEEE Transactions on Ultrasonics, Ferroelectrics, and Frequency Control* **55**.9 (2008), 2104–2108.
- [9] H. Wu et al. A novel two-degrees-of-freedom piezoelectric energy harvester. *Journal of Intelligent Material Systems and Structures* **24**.3 (2013), 357–368. DOI: 10.1177/1045389X12457254.
- [10] L. G. H. Staaf et al. Modelling and experimental verification of more efficient power harvesting by coupled piezoelectric cantilevers. *Journal of Physics: Conference Series* **557** (2014). DOI: 10.1088/1742-6596/557/1/012098.
- [11] A. Vyas. Personal communication. Chalmers University of Technology, Department of Microtechnology and Nanoscience, May 19, 2020.
- [12] A. Vyas. Personal communication. Chalmers University of Technology, Department of Microtechnology and Nanoscience, Feb. 19, 2020.
- [13] Z. Song and C. Su. Computation of Rayleigh Damping Coefficients for the Seismic Analysis of a Hydro-Powerhouse. *Shock and Vibration* (2017). DOI: 10.1155/2017/2046345.
- [14] P. Lundgren. Personal communication. Chalmers University of Technology, Department of Microtechnology and Nanoscience, May 12, 2020.
- [15] D. Shen et al. The design, fabrication and evaluation of a MEMS PZT cantilever with an integrated Si proof mass for vibration energy harvesting. *Journal of Micromechanics and Microengineering* **18**.5 (2008).



CHALMERS
UNIVERSITY OF TECHNOLOGY